University of Cambridge
Department of Engineering

Masters Project Report

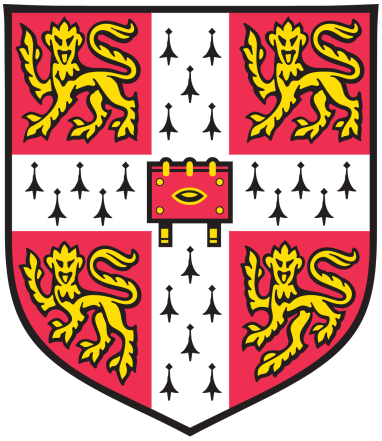


# Propulsion Systems for [small?] VTOL Electric Vehicles

**Jordan Sandberg Eriksen**

Supervised by: **Dr Sam Grimshaw**

**Abstract**

Abstract here..

# Contents

| | | |
|---|---|---|
| Electric Vertical Take-Off and Landing | e-VTOL | |
| Flying Test-Bed | FTB | |
| Axial Flow Velocity | $V_x$ | |
| Fan Speed | $\Omega$ | |
| Fan Hub Radius | $r_h$ | |
| Fan Casing Radius | $r_c$ | |
| Fan Mid-line Radius | $r_m$ | |
| Mid-line Fan Speed | $U$ | $= \Omega \cdot r_m$ |
| | | |
| Flow Coefficient | $\phi$ | $= \frac{V_x}{U}$ |
| Stage Loading | $\psi$ | $= \frac{\Delta h_0}{U^2}$ |

# Nomenclature

e-VTOL Test
FTB Test
$V_x$ Axial flow velocity
$\Omega$
$r_h$
$r_c$
$r_m$
$U$
$\phi$ Flow coefficient
$\psi$ Stage loading

# Introduction

Intro and motivation

Consider Heilmeier when structuring this section.
- Integrate battery into casing, increase payload volume/utilise space

## 1.1 Literature Review

## 1.2 Research Questions

## 1.3 Approach

High level overview of what's been done and how the report is set out.

# Flying Test Bed and Propulsor Design

## 2.1 System Design

### 2.1.1 Flying vehicle development

A UROP was conducted in the summer preceding this project during which an axi-symmetric quadcopter flying test bed was designed and tested. The two challenges addressed were structural design of the chassis, and the customisation of flight control hardware and software. The UROP concluded with successful hover testing of the flying test bed. Off-the-shelf $10in.$ propellers were used in the test[1].

**Mechanical design**
The test bed was designed to be rapidly 3D printable, light weight – whilst maintaining

[1] REFERENCE UROP REPORT

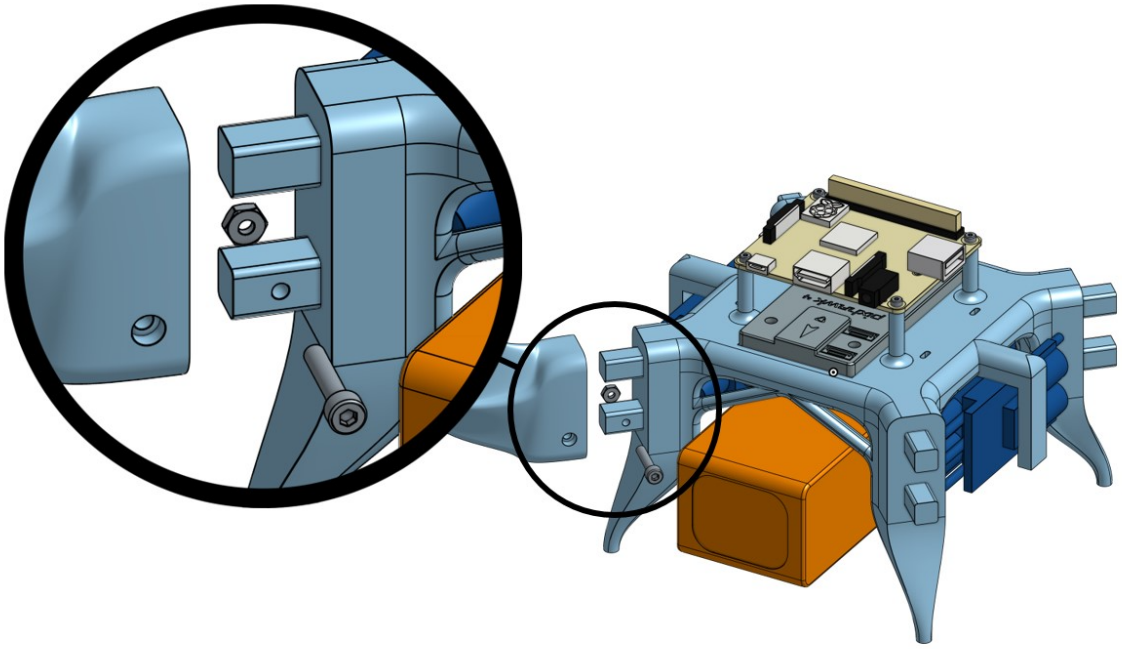

Figure 1: Flying test bed chassis showing exploded detail of double mortise and tenon joint for propulsor arms

structural integrity – and modular to allow various propulsors and instrumentation to be mounted. Instrumentation management and flight hardware are mounted on a central chassis that is 3D printed as one piece for rigidity and to reduce complexity. Cantilevered propulsor arms are attached to the central chassis with a double mortise and tenon style mount, fastened by one M3 cap-head as in Fig. 1. Modularity allows for design iteration and rapid part replacement if required.

The following hardware is mounted directly onto the central chassis:

- ***Pixhawk* 4 Flight Control hardware** – Packaged, customizable autopilot hardware
- **PM07 Power Module** – Power module managing distribution of power from battery/power supply to flight controllers, other on-board computers, and motors
- **Raspberry Pi 3 Model A+** – On-board computer managing data acquisition and assisting flight controller automation
- ***ADCPi* ADC Breakout** – Analogue to digital converter mounted directly to the Rasperry Pi 3
- **4x *Aerostar* 50A ESC** – Electronic Speed Controller driving BLDCM motors
- **Optional: *Turnigy* 5000mAh 14.8V (4-cell) Battery** – Large capacity 14.8V (nominal) battery. Can be replaced by a tethered 12V power supply.

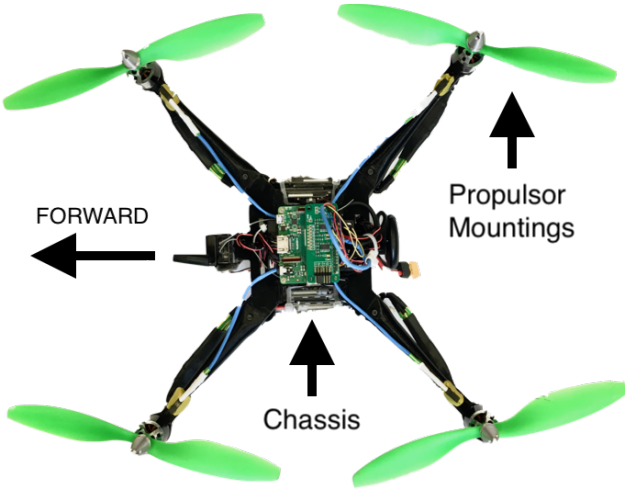


Figure 2: Image of flying test bed with propellers attached

The central chassis has dimensions of approximately $125mm$ x $139mm$ x $93mm$ (see Fig. 10). It has a dry mass (excluding battery) of $0.529kg$ and the battery has a mass of $0.466kg$.

**Customisation of *Pixhawk 4* flight hardware/software**
Pixhawk 4 is a packaged flight control hardware system running open source PX4 firmware. Interaction with the system is via the GUI QGroundControl and either a wireless telemetry transmitter-receiver pair or a serial connection (such as a USB). QGroundContol allows a predetermined automated flight path to be followed or alternatively the hardware can be configured to allow manual control provided adequate control inputs can be provided (a 16-channel remote with an 8-channel PPM-PWM converter is used here). The PM4 firmware includes various airframe configuration profiles, enabling it to adapt to the vehicle configuration and motor layout. The flying test bed is configured as a symmetric 'X' quadcopter. The profile was tuned to the flying test bed by varying PID gains on the control software, ensuring stable operation in hover. It provides a stable hover mode that is intended to reduce horizontal position deviation and maintain a fixed altitude. This means only small corrective inputs are required from the operator to ensure near stationary hover even in enclosed environments. It was found however that wall effects can be significant and so care must be taken when operating in such environments.

### 2.1.2 Subsystem Functions

**Raspberry Pi 3 Model A+ (RPi3)**
The RPi3 is a light-weight, small-footprint, 64-bit quad-core processor with UNIX-based operating system and Wi-Fi connectivity that can be run 'blind' through an SSH connection from a remote machine. It provides data acquisition and on-board data processing in Python and is used to pre-process test data before wirelessly transferring it back to the

remote machine. RPi3 has 28 general purpose input/output (GPIO) pins as well as $I^2C$ and serial interfaces among others.

**ADCPi ADC Breakout**
The ADC breakout board is designed specifically for the RPi3. Operating through the $I^2C$ interface, each breakout board provides an 8-channel ADC at 11 to 17 bit resolution with sample rates of 240 to 3.75 *samples/sec* respectively.

**PM07 Power Module**
Designed to operate in tandem with the Pixhawk 4 flight controller, the PM07 provides power control for all the high-power outputs (such as the motors) as well as a regulated 5V output for the flight controller and RPi3. Power input is 7-51V DC and the output current is limited to 120A (approximately 30A per propulsor). The battery selected can operate up to 125A to accommodate this demand. PM07 also provides 2 ADC inputs.

### 2.1.3 Subsystem Interaction

Pixhawk 4 provides simple subsystem interaction through it's input ports. 5 ports connect the flight controller to the power module: 2x power inputs, 1x motor PWM outputs, 1x auxilary PWM output, and 1x ADC input. The serial port on the Pixhawk 4 is rewired to connect to the RPi3's UART TXD and RXD terminals (Fig.9 shows all connections made to the RPi3 header). The $I^2C$ port connects to an $I^2C$ bus that allows up to 5 devices to interface with the Pixhawk 4, including 3 ultrasound sensors measuring proximity in the x, y, and z directions. These sensors can optionally be connected via the ADC for use by the RPi3. Figure 3 shows schematically how the subsystems interact.

### 2.1.4 Telemetry

**Pixhawk 4 wireless telemetry**
The plug-and-play telemetry module allows wireless connection to the Pixhawk 4 from a ground control station on a remote machine such as QGroundControl. This is used to communicate with the Pixhawk 4 about flight control and to log power usage data (PM07 voltage and current output).

**SSH/SCP on RPi3**
RPi3 is wireless enabled allowing it to be accessed remotely via the SSH (secure shell) protocol. SCP (secure copy protocol) allows files to be copied to and from the RPi3. This is used after data collection to collect all data on the remote machine. A dedicated wireless router is used to connect the RPi3 to a remote machine – done automatically on start-up of the RPi3.

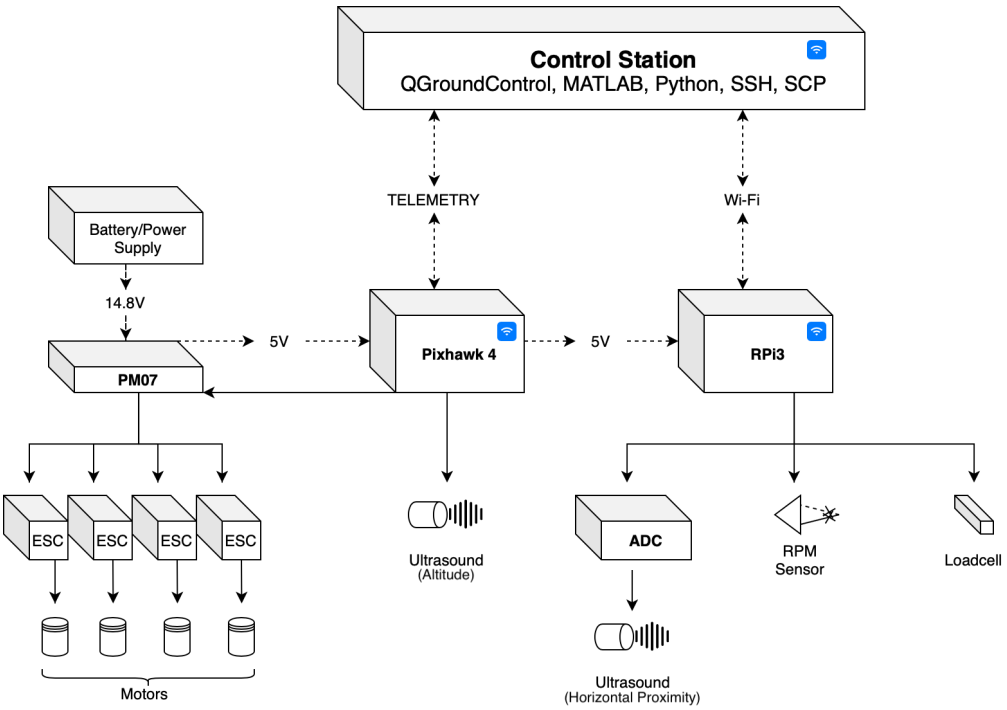


Figure 3: Subsystem schematic of flying test bed

## 2.2 Aerodynamic Design

The aerodynamic design of an electric ducted fan, 3D printed in PLA, is described below. The flying test bed is powered by 4 ducted fans and is required to be able to achieve a steady hover with a payload equal to the weight of the flying test bed chassis. Figure 4 shows an overview of the ducted fan configuration with design variables labelled where appropriate.

### 2.2.1 Figure of Merit and Design Point

A low-speed (incompressible) ducted fan in hover fundamentally differs from both a propeller and a ducted fan in high-speed free stream velocity. A propellers exit static pressure is approximately equal to atmospheric, however a low-speed ducted fan can vary it's exit pressure by varying the diffusion factor, $\sigma$, defined as the ratio of exit flow area ($A_e$) and blade passage flow area ($A_x$), as in Eqn. 1.

$$\sigma = \frac{A_e}{A_x} \tag{1}$$

As the exit static pressure must be approximately atmospheric, assuming the diffuser flow remains attached variation in $\sigma$ will result in a variation in $p_x$, the blade passage static pressure.

A ducted fan in non-zero free stream velocity is required to reduce frontal area in order to decrease aerodynamic drag, however a ducted fan in static hover is not. This means the

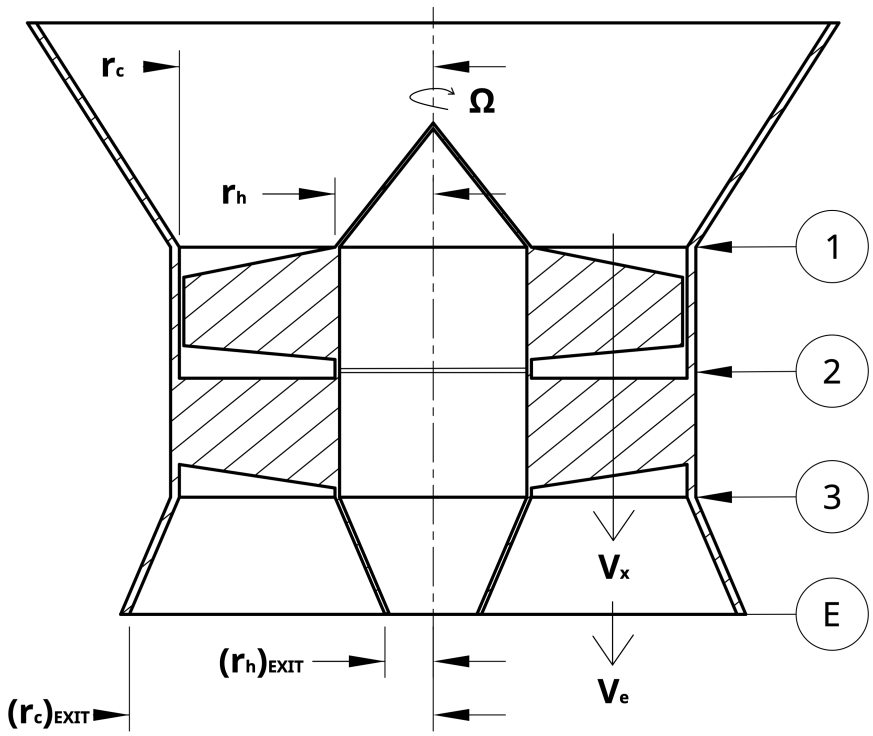


Figure 4: Configuration of ducted fan. **1:** Inlet plane; **2:** Inter-rotor-stator plane; **3:** Stator exit plane; **E:** Diffuser exit plane.

addition of a diffuser to reduce exit velocity – increasing efficiency – does not come at the cost of drag.

**Figure of Merit:**[2] The effectiveness of a propulsor in hover can be measured by the figure of merit, $M_F$, defined as a non-dimensional thrust-to-power ratio (Eqn. 2).

$$M_F = \frac{T}{P}\sqrt{\frac{T}{2\rho A_x}} \tag{2}$$

Considering a large control volume ($V_{in} \approx 0$) around a simple ducted fan, treating the blade plane as a stagnation pressure actuator disk and the exit static pressure as atmospheric allows the theoretical thrust to be determined. This can then be written in terms of the blade passage quantities ($A_x$, $V_x$ etc) and the diffusion factor, $\sigma$, using continuity.

$$T = \dot{m}V_e = \rho A_e V_e^2 \qquad \textit{by continuity...} \qquad \therefore T = \frac{\rho A_x V_x^2}{\sigma} \tag{3}$$

Theoretical power requirement can be determined by the rate of transfer of kinetic energy to the flow.

[2]REFERENCE PERIERA

$$P = \frac{1}{2}\dot{m}V_e^2 \qquad \textit{by continuity...} \qquad \therefore P = \frac{\rho A_x V_x^3}{2\sigma^2} \tag{4}$$

Substituting Eqn. 3 and Eqn. 4 into Eqn. 2 gives the result in Eqn. 5.

$$M_F = \sqrt{2\sigma} \tag{5}$$

Hence to maximise hover performance the diffusion factor must be maximised. This necessitates a high performing diffuser with a minimised mass. Due to the negative effects of an adverse pressure gradient on flow attachment (and effective flow area) in a diffuser, the required length of a diffuser flow that remains attached will increase non-linearly with diffusion factor[3]. This trade-off between performance and weight limits the design choice of diffusion factor to avoid prohibitively heavy propulsors. Section 2.2.2 discusses this problem. This result also shows that a diffusion factor of 1, that is to say with no diffusion downstream of the blades, the theoretical figure of merit is $M_F = \sqrt{2} \approx 1.414$. Periera 2008[4] shows the maximum theoretical figure of merit for a propeller to be 1, therefore provided the diffusion factor remains above 0.5, fan figure of merit should be great than propeller performance in hover.

**Non-dimensional Operating Point:** The design of both the rotor and stator fan blades can be determined by the choice of non-dimensional operating point given by flow coefficient (Eqn. 6(a)) and stage loading (Eqn. 6(b)) where the mid-line blade velocity is $U = \Omega \cdot r_m$ with $r_m$ equal to the mid-line radius.

$$\phi = \frac{V_x}{U} \quad (a) \qquad\qquad \psi = \frac{\Delta h_0}{U^2} \quad (b) \tag{6}$$

Assuming isentropic flow, stage loading can be written in terms of the stagnation pressure rise, $\Delta p_0$. Using Bernoulli and assuming exit static pressure is equal to atmospheric therefore gives an expression for $\Delta h_0$ in terms of the exit velocity $V_e$.

$$\Delta p_0 = (p_0)_e - (p_0)_{in} = (p_e + \frac{1}{2}\rho V_e^2) - p_a$$

$$\Delta p_0 = \frac{1}{2}\rho V_e^2$$

$$\therefore \Delta h_0 = \frac{\Delta p_0}{\rho} = \frac{1}{2}V_e^2 = \frac{V_x^2}{2\sigma^2} \tag{7}$$

Therefore $\phi$, $\psi$, and $\sigma$ are determined by Eqn. 8

[3]REFERENCE ESDU
[4]REFERENCE PERIERA

$$\sigma^2 = \frac{\phi^2}{2\psi} \tag{8}$$

The choice of operating point therefore sets the diffusion factor and consequently the theoretical figure of merit of the propulsor. Section 2.2.2 considers the interaction between the operating point and geometric variables, and the subsequent impact of required performance, whilst section 2.2.3 considers the embodiment of the design point into 3D rotor and stator blades.

**Estimation of Operating Fan Speed:** Equation 5 shows the effectiveness of a ducted fan in hover is independent of the speed of rotation of the fan. The fan speed however does impact the magnitude of the thrust developed, shown by substituting Eqn. 6(a) into Eqn. 3.

$$T = \frac{\rho A_x (\Omega r_m \phi_m)^2}{\sigma} \tag{9}$$

Equation 9 shows thrust to vary with both fan speed and fan size, and so the required thrust will vary depending on the choice of these parameters. The effect of fan size is discussed in section 2.2.2.

.

.
*****NOTES ON SECTION*****
ESDU diffusion tables?

### 2.2.2 Mid-line Blade Design

**Mid-line Location:** Maximising the flow area for a given propulsor radius ensures minimum use of material and therefore a lighter design. This results in a small hub radius ($20mm$) and consequently very low hub-to-tip ratios compared to conventional compressors. As a result, selecting a mid-line at the mean radius introduces large differences in mass flow above and below the mid-line. This results in large variations in loading across the span. The alternative mid-line location is based on balancing the mass flow above and below the mid-line. This sets the mid-line radius at the root-mean-square off the hub and tip radii, as in Eqn. 10.

$$r_m = \sqrt{\frac{r_h^2 + r_c^2}{2}} \tag{10}$$

**Overall Performance:** As shown in section 2.2.1 the overall characteristics such as thrust and power can be determined from the fan geometry and the mid-line non-dimensional quantities $\phi_m$ and $\psi_m$. Equation 5 suggested a larger diffusion factor will increase performance, however due to the difficulty of diffusing flow, the length of the diffuser required to enable large diffusion factors can be prohibitive. Further, on transition from static hover to horizontal flight a long diffuser will generate considerable drag due to its large flow facing area.

A problem therefore arises when determining the required thrust. For steady hover, thrust must equal the weight of the vehicle. However as the design thrust varies, as does the weight, creating a circular problem. In order to solve this a mass model is required that, given the propulsors operating point, estimates it's weight.

The variables required to define both the weight and performance of a ducted fan are outlined in table 1.

Table 1: Variables defining propulsor weight and performance

| | |
|---|---|
| $r_c$ | Blade passage casing radius |
| $r_h$ | Blade passage hub radius |
| $\Omega$ | Rotor angular velocity |
| $\sigma$ | Diffusion factor |
| $\phi_m$ | Mid-line flow coefficient |
| $\psi_m$ | Mid-line stage loading |

A notable exclusion from this list is the length of the diffuser, however the lower limit of this value is estimated from ESDU 75026:Figure 3[5] which gives empirical limits of diffuser lengths for symmetric annular diffusers. Therefore the length of the diffuser is determined by correlating the appropriate values from $r_c$, $r_h$, and $\sigma$ to the ESDU data.

Equations 3 and 4 can be expressed in terms of the variables in tab. 1 as follows

$$T = \frac{\rho\pi\phi_m^2\Omega^2(r_c^4 - r_h^4)}{2\sigma} \tag{11}$$

$$P = \rho\pi\phi\psi\Omega^3(r_c^2 - r_h^2)\left(\frac{r_c^2 + r_h^2}{2}\right)^{\frac{3}{2}} \tag{12}$$

Equation 11 can be equated to the vehicle weight to determined the variables required for hover. A mass model is developed to enable this.

**ESDU 75026 Diffuser Data:** ESDU 75026 presents the performance of circular annular diffusers in incompressible flow.

$$C_{pr} = \frac{p_e - p_x}{\frac{1}{2}\rho V_x^2} \tag{13}$$

ESDU 75026:Figure 3 shows the line of $C_{pr}^{**}$ representing the length ratio at which $C_{pr}$ (Eqn. 13) is maximised for a given area ratio. This allows a minimum diffuser length to be determined for a given area ratio and upstream span $(r_c - r_h)$. This line can be approximated with an R-squared value of 0.9999 by

[5]REFERENCE ESDU TABLES HERE

$$\frac{L}{r_c - r_h} = -5.56\sigma^3 + 24.16\sigma^2 - 23.41\sigma + 5.413 \tag{14}$$

**Mass Model – Diffuser:** The diffuser hub and casing are modelled as a hollow truncated cone 3D printed in PLA with height $L$ (determined by Eqn. 14), a base radius $r_h$ (for the hub) and $(r_c)_{EXIT}$ (for the casing), a truncation radius of $(r_h)_{EXIT}$ (for the hub) and $r_c$ for the casing, and a thickness $t$, as in Fig. 5. Equation 15 gives the volume of a hollow truncated cone with the respective values of $R$, $r$, $S$, and $s$ for the hub and casing defined in tab. 2.

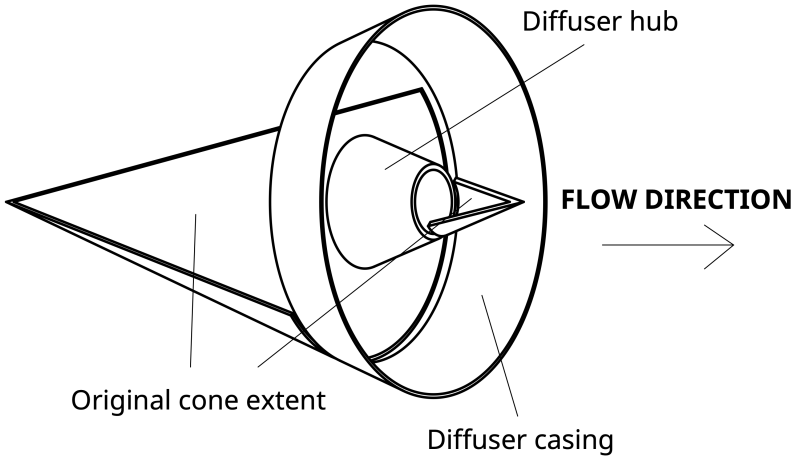


Figure 5: Hollow truncated cone diffuser model showing original extent of cone before truncation

$$V = \frac{h\pi}{3}(R^2 + Rr + r^2 - S^2 - Ss - s^2) \tag{15}$$

$$m_{DIFF.} = \rho_{PLA}(V_{HUB} + V_{CASE}) \tag{16}$$

From the ESDU data, a annulus flow with uniform axial velocity is diffused in the shortest distance if the diffuser is symmetric such that the diffuser angle at casing and hub is equal giving

$$\frac{(r_c)_{EXIT} - r_c}{L} = \frac{r_h - (r_h)_{EXIT}}{L} \tag{17}$$

Applying Eqn. 17 and expanding Eqn. 1 in terms of radius, the diffuser exit hub and casing radii can be determined.

$$(r_h)_{EXIT} = \frac{r_c + r_h}{2} - \frac{\sigma}{2}(r_c - r_h) \tag{18}$$

| | Hub value | Casing value |
|---|---|---|
| **R** | $r_h$ | $(r_c)_{EXIT} + t$ |
| **r** | $(r_h)_{EXIT}$ | $r_c + t$ |
| **S** | $r_h - t$ | $(r_c)_{EXIT}$ |
| **s** | $(r_h)_{EXIT} - t$ | $r_c$ |
| **h** | $L$ | $L$ |

Table 2: Parameter values for diffuser hub and casing

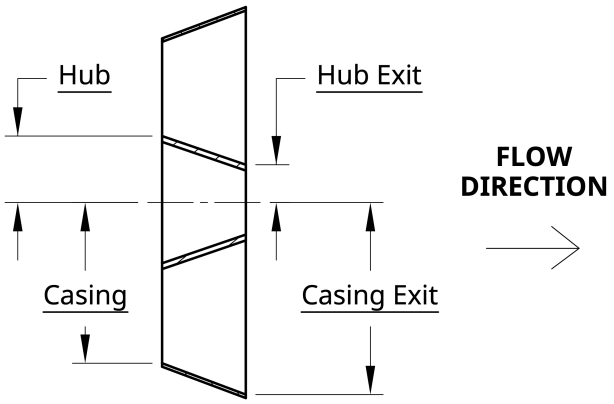


Figure 6: Dimensions of hollow truncated cone diffuser model

$$(r_c)_{EXIT} = \frac{r_c + r_h}{2} + \frac{\sigma}{2}(r_c - r_h) \tag{19}$$

Substituting Eqn. 18 and Eqn. 19 into Eqn. 15, Eqn. 16 can be solved to approximate the mass and therefore the weight of a diffuser at a particular set of design parameters.

**Mass Model – Blade Passage:** The blade passage (excluding rotor and stator) are modelled as a straight annulus 3D printed in PLA. The passage itself has inner radius $r_h$ and outer radius $r_c$. The casing is modelled to have thickness of $t_c = 1.5mm$ and the hub section has a thickness of $t_h = 5mm$. The length of the blade passage is $L_{BP} = 70mm$ giving a volume of

$$V_{BP} = L_{BP}\pi[2r_h t_h - t_h^2 + 2r_c t_c + t_c^2] \tag{20}$$

Multiplying by the density of PLA gives the mass of the blade passage section, which can be written in terms of the unknown variable $r_c$ and $r_h$

$$m_{BP} = 2.73r_h + 0.818r_c - 0.0062 \tag{21}$$

**Mass Model – Intake:** For simplicity the intake is also modelled as a hollow truncated cone, an approximation for it's actual ellipsoidal geometry. It has approximately equal length to it's change in radius which is set approximately equal to the blade passage span, $r_c - r_h$. Therefore using Eqn. 15, and assuming a thickness of $1mm$, the intake mass can be approximated by

$$m_{IN.} = 3.90(r_c - r_h)(3r_c - r_h + 0.001) \tag{22}$$

**Mass Model – Blades:** As the number of blades has not yet been determined, the blades are modelled as having the equivalent mass of a annular flat disk of thickness $t_{ROTOR} = 1.5mm$ for the rotor and $t_{STATOR} = 3mm$ for the stator. The resulting mass is given by

$$V_{BLADES} = \pi(r_c^2 - r_h^2)(t_{ROTOR} + t_{STATOR}) \tag{23}$$

$$m_{BLADES} = 17.5(r_c^2 - r_h^2) \tag{24}$$

**Thrust = Weight:** The mass model described above provides an approximation for the mass of a particular design based on the design parameters listed in tab. 1. In hover, the load carried by each propulsor is equal to the propulsor's weight and its share of the payload weight (4 propulsors). The payload here is the flying test bed chassis and battery, described in section 2.1.1. Using Eqn. 11 the thrust developed can be set equal to the required thrust to give the relationship between the design variables when the propulsor is operating in the static hover state.

$$T = g\left[m_{PROPULSOR} + \frac{m_{CHASSIS}}{4} + \frac{m_{BATTERY}}{4}\right] \tag{25}$$

$$\frac{\rho\pi\phi_m^2\Omega^2(r_c^4 - r_h^4)}{2\sigma} = g[m_{DIFF.} + m_{BP} + m_{IN.} + m_{BLADES}] + 2.44N \tag{26}$$

**Reduction of Unknown Variables:**
In order to solve the design problem, the number of unknowns must be reduced. This is achieved by fixing the propulsor size. The application demonstrated here is for a small quad-copter style vehicle. Furthering work carried out by Jonny 2019[6] in which the performance of a ducted fan was determined with $M_F > 1$ and $r_c = 120mm$, this design is to be scaled by a half giving

$$r_c = 60mm \tag{27}$$

The value of $r_h$ is determined by the outer diameter of the electric motor used to drive the rotor. This is typically $d < 35mm$, therefore $r_h$ is chosen to be

$$r_h = 20mm \tag{28}$$

Giving a hub-to-tip ratio of 0.333. This leaves diffusion factor, $\sigma$, and the rotor angular velocity, $\Omega$. The relationship between the design parameters $\phi$, $\psi$, and $\sigma$, as well as the

[6]CUED 4th Year Project Report June 2019

relationship between diffuser length and $\sigma$, results in a limit on the design point due to the requirement for diffuser length, $L_{DIFF.}$, to not become prohibitive (as discussed in sec. 2.2.2: *Overall Performance*). This is limited to $L_{DIFF.} \leq 100mm$. Therefore from Eqn. 14

$$-5.56\sigma^3 + 24.16\sigma^2 - 23.41\sigma + 5.413 \leq 2.5 \tag{29}$$

$$\therefore \sigma \leq 1.2 \tag{30}$$

It should be noted that this limit on $\sigma$ arises from the performance of a conventional circular annular diffuser, as presented in ESDU 75026. This limit may be exceeded however through the use of various flow devices, such as splitter vanes. These ideas are discussed further in the future work section (sec. 5) and are not implemented here. With the other parameters set, the thrust = weight condition sets the value of $\Omega$ at each design point. The required motor speed impacts the choice of electric motor used as the maximum efficiency range will vary.

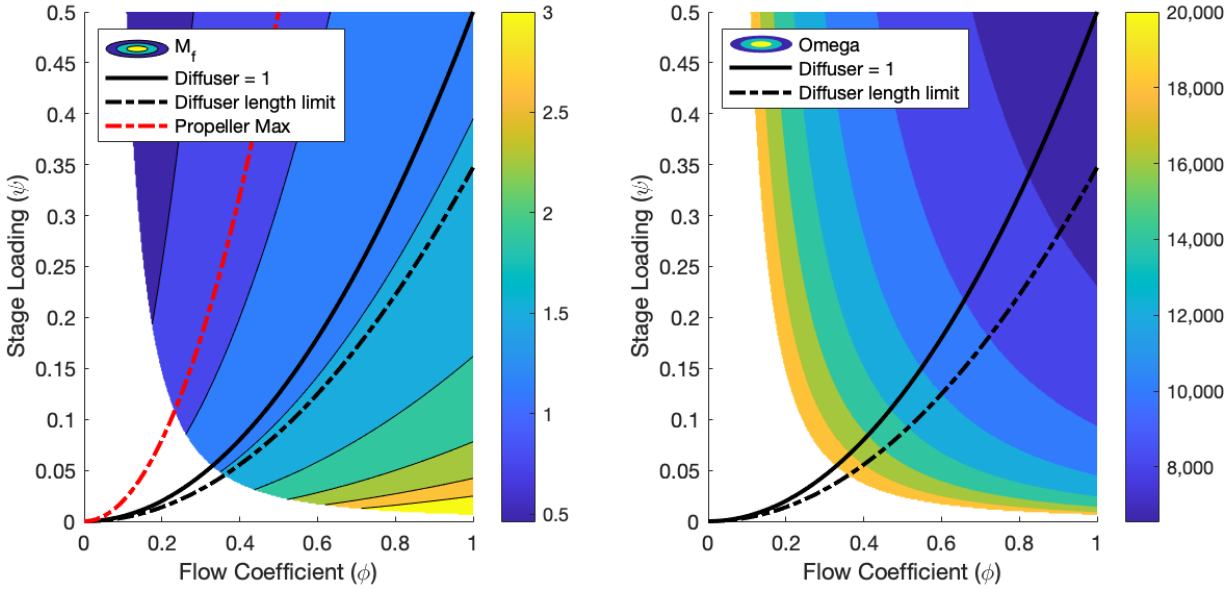


(a) Figure of merit as a function of $\phi$ and $\psi$

(b) Motor speed in RPM as a function of $\phi$ and $\psi$ satisfying hover condition of thrust = weight

Figure 7: Contour plots of the $\phi$-$\psi$ design space generated using mass model. Plots display the diffuser limit arising from a maximum diffuser length, and the line representing a diffusion factor of 1.

Figure 7a shows the variation in figure of merit across the design space. The diffuser length limit considerably constrains what sections of the design space are accessible, regardless the majority of the design space provides significantly better hover performance than a propeller. Figure 7b shows the variation in required motor speed (in RPM) across the

design space. The required motor speed is very high, which sets the requirement for the electric motor to have an optimum efficiency at around $7,000 - 12,000$ RPM. In order to reduce motor size the lower end of this range is chosen (this is discussed in more detail in Section 2.4) therefore

$$\Omega = 8500 \text{ RPM} \tag{31}$$

SOMEONE 20XX[7] shows suitable range for flow coefficient in incompressible turbomachinery to not exceed 0.8, and stage loading to not exceed 0.3. Considering Fig. 7b a line of constant RPM at approximately 8500 RPM in the region between the two diffuser limits passes from top-left to bottom-right. Figure 7a shows figure of merit to increase towards the bottom-right and so to satisfy all the conditions above and maximise figure of merit, an operating point is chosen and is tabulated in Table 3.

Table 3: Propulsor design point

| | |
|---|---|
| $r_c$ | $60mm$ |
| $r_h$ | $20mm$ |
| $\Omega$ | 8500 RPM |
| $\sigma$ | 1.1314 |
| $\phi_m$ | 0.80 |
| $\psi_m$ | 0.25 |

Conventional propulsive turbomachines, such as high bypass ratio turbo-fans must limit their flow coefficient as this comes at the cost of propulsive efficiency. The propulsor considered here however differs from this as it diffuses the exit flow, reducing it's velocity and therefore reducing exit loss.

### 2.2.3 3D Blade Design

Overall performance has been determined by setting the mid-line values of flow coefficient, $\phi_m$, and stage loading, $\psi_m$. The values of $\phi$ and $\psi$ must vary along the span as the local value of blade speed changes, and for equilibrium to be maintained across the flow passage. In order to satisfy these conditions the radial equilibrium equation must be satisfied. Potential solutions to this equation are discussed below.

**3-dimensional Flow Solutions to Radial Equilibrium:** Radial equilibrium states that for axi-symmetric and incompressible annulus flow Eqn. 32 must be satisfied.

$$\frac{dh_0}{dr} - T\frac{ds}{dr} = V_x\frac{dV_x}{dr} + \frac{V_\theta}{r}\frac{d(rV_\theta)}{dr} \tag{32}$$

[7]REFERENCE SMITH CHARTS? LOOK AT WHY LIMITING PSI and PHI

Assuming there is no variation in stagnation enthalpy or entropy across the span, this reduces to

$$V_x \frac{dV_x}{dr} + \frac{V_\theta}{r}\frac{d(rV_\theta)}{dr} = 0 \tag{33}$$

Noting Eqn. 6 and applying Euler's work equation, we obtain

$$\phi r \frac{d(\phi r)}{dr} + \psi \frac{d(\psi r^2)}{dr} = 0 \tag{34}$$

Which has general solutions in the form

$$\phi = \phi_m \Big(\frac{r}{r_m}\Big)^A \quad (a) \qquad\qquad \psi = \psi_m \Big(\frac{r}{r_m}\Big)^B \quad (b) \tag{35}$$

Where $\phi_m$ and $\psi_m$ are the mid-line quantities. Substituting eqns.35a & 35b into Eqn. 34 gives[8]

$$\left[\phi_m \Big(\frac{r}{r_m}\Big)^A\right]^2 (1+A) = -\left[\psi_m \Big(\frac{r}{r_m}\Big)^B\right]^2 (2+B)$$

$$\therefore \phi^2(1+A) = -\psi^2(2+B) \tag{36}$$

This solution can be used to determine the values of the exponents, $A$ and $B$. The constant $B$ is referred to here as the vortex distribution exponent as it determines the tangential velocity variation in the $r$-$\theta$ plane.

**Free Vortex (B = -2):** One such distribution arises from the free vortex condition. This results from the solution to Eqn. 36 in which both LHS and RHS are equal to zero giving

$$A = -1 \quad (a) \qquad\qquad B = -2 \quad (b) \tag{37}$$

Therefore from Eqn. 35a and Eqn. 37a

$$\phi(r) \sim \frac{1}{r} \qquad\qquad \therefore \frac{d}{dr}(V_x) = 0 \tag{38}$$

Therefore axial velocity across the span must be constant. Similarly it can be shown from Eqn. 35b and Eqn. 37b

$$\psi(r) \sim \frac{1}{r^2} \qquad\qquad \therefore \frac{d}{dr}(\Delta h_0) = 0 \tag{39}$$

Therefore the loading is equal across the span. It can then be determined that $V_{\theta 2} \sim 1/r$ resulting in a vorticity free (lowest loss) flow[9]. Both the constant $V_x$ and the constant $\Delta h_0$

[8]STICK THE DERIVATION IN AN APPENDIX????

[9]REFERENCE DIXON AND HALL FLUID MECHANICS AND THERMODYNAMICS OF TURBOMACHINERY, CHAPTER 6.3, P218

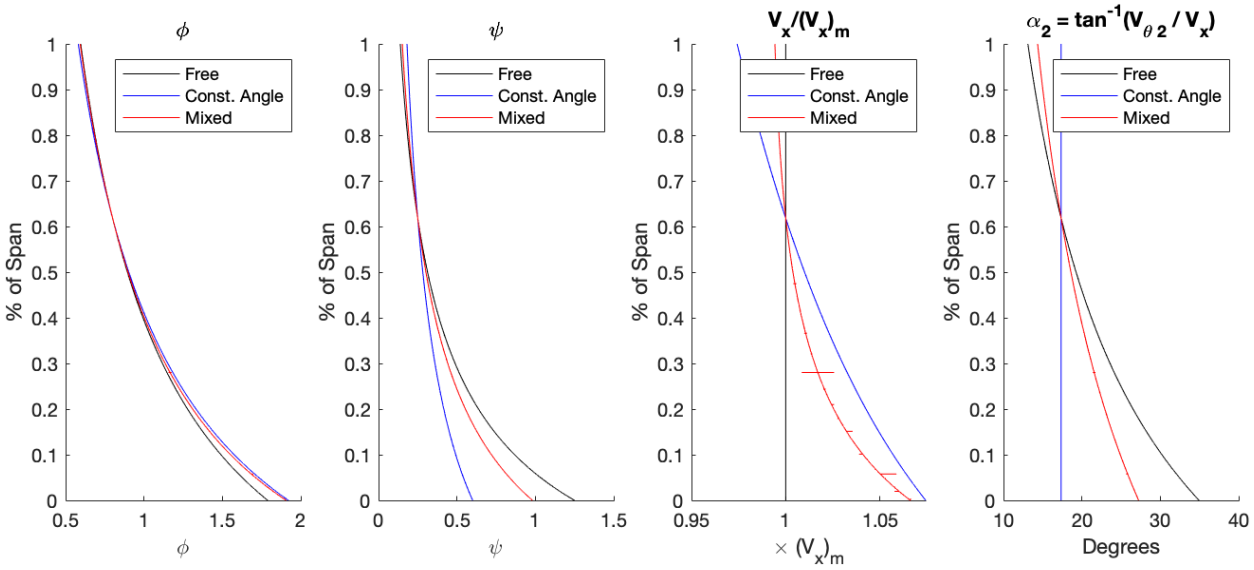


Figure 8: Distributions of design parameters $\phi$ and $\psi$ and non-dimensionalised axial and tangential velocities, $V_x$ and $V_{\theta 2}$ respectively, across the span at 3 different boundary conditions (free vortex, constant angle and mixed vortex).

conditions indicate uniform exit static pressure. In practice the variation in $V_{\theta 2}$ across the span results in large variations in blade twist angle that can reduce efficiency (see Fig. 8 that shows $V_{\theta 2}$ variation resulting in over $20^o$ of absolute flow angle variation).[10]

Furthermore, Fig. 8 shows stage loading, $\psi$, to become larger than 1 at radii close to the hub. From Euler, and given axial inlet flow

$$\Delta V_\theta = V_{\theta 2} = \psi U \tag{40}$$

This shows the tangential velocity at the hub to be greater than the local blade speed. By reducing the value of the vortex distribution exponent, $B$, this can be avoided by keeping $\psi \leq 1$.

**Mixed Vortex ($-2 \leq B \leq 0$):** Equation 36 can also be used to numerically solve the radial equilibrium equation for any value of the vortex distribution exponent provided $\phi_m$ and $\psi_m$ are known. A summary of vortex distribution exponent values is shown n tab. 4. The mixed vortex design shown in Fig. 8 has a vortex distribution exponent of 1.7. This produces a vortex distribution that, at the hub, has a tangential velocity is equal to the velocity of the hub wall. This reduces the absolute velocity of the flow past the wall and therefore minimises frictional loss for a given axial velocity.

**Constant Angle:** Another common design is for constant absolute flow angle across the span, such that

[10] AGAIN NEED A REFERENCE FOR THIS?

$$\frac{d}{dr}\left(\frac{V_\theta}{V_x}\right) = 0 \tag{41}$$

$$\therefore \frac{\psi}{\phi} = constant\left( = \frac{\psi_m}{\phi_m}\right) \tag{42}$$

This results in the exponents A and B being equal giving

$$A = B = -\left(\frac{2\psi_m^2 + \phi_m^2}{\psi_m^2 + \phi_m^2}\right) \tag{43}$$

Table 4: Vortex distribution exponents for various boundary conditions

| | Free Vortex $V_x(r) = const.$ | Constant Angle $V_x/V_\theta = const.$ | $B = ...$ see Eqn. 36 |
|---|---|---|---|
| **A** | -1 | $-\left(\frac{2\psi_m^2+\phi_m^2}{\psi_m^2+\phi_m^2}\right)$ | *Solve numerically* |
| **B** | -2 | $-\left(\frac{2\psi_m^2+\phi_m^2}{\psi_m^2+\phi_m^2}\right)$ | *Solve numerically* |

The relative merits of each of the vortex distributions are discussed in Section 4.1.1 in which the three designs presented here are tested.

**Blade Number:** Lieblein [REFERENCE FROM DIXON AND HALL GET THE ORIGINAL LIEBLEIN REFERENCE] presents a correlation for diffusion factor as a function of velocities and the pitch-chord ratio of the blades.

Blade number

- Correlation say this - This is how you get blade number - Problems with correlations - Different design region? Is the correlation valid? - Examples of large variation in chord and weirdness - Impact of vortex distribution (dashboard) - Choice of DF - Variable DF? - Improved pitch-chord

Deviation

- Correlations say this - This is how you get deviation - Problems with correlation (illustrate with dashboard blade) - Impact of vortex distribution - Impact of DF - Improved deviation - Fixed deviation design?

Sweep/Lean

- Reference JVT - Obtuse angles at tip and hub - Sweep to reduce size of design

Profiles
- Where did they come from? - What are they? - How are they implemented?
Blade design code
- How does all this fit together?

## 2.3 Mechanical Design

### 2.3.1 Mass Model/Propulsor Dimensions

.
.
*****NOTES ON SECTION*****

Thrust = Weight condition
Mass model to close the problem

### 2.3.2 Shroud Tip Clearance

Shroud thickness
FEA
3D printer tolerances

### 2.3.3 Hollow Stators

Power supply
Weight reduction
Tolerance
How to

### 2.3.4 3D Printing

Printer used
Printer tolerance
Design adjustments to enable good printing
- Straight TRAILING edge
- Raft and reduce air-gap

## 2.4 Electrical Design

### 2.4.1 Choice of Electric Motor

Size ($d < 36mm$)

### 2.4.2 Power vs Torque Design Space

### 2.4.3 Power Supply

Want to simulate using a battery pack for actual flight conditions but increase run-time. Choose 12V steady state operating voltage (14.8V nominal Li-Po).

### 2.4.4 Instrumentation Design

Maybe reference here but give details in the appendix? Described more in section 3.2.2 RPM
Thrust
- Calibration
Power
Pressures

# Methods

## 3.1 Experiments

### 3.1.1 Stationary Propulsor Test

Setup
- Stand
Test variables
- Speeds
- Sigma
- Rotor design

### 3.1.2 Flying Test Bed

## 3.2 Experimental Method & Data Processing

### 3.2.1 Non-dimensional Quantities

Pressure quantities, FOM, $\phi$, $\psi$.

#### 3.2.2 Instrumentation

Power (DC Current and Voltage), Thrust, FOM, RPM, Pressures

#### 3.2.3 Data Acquisition

Acquisition and integration of systems and software.

#### 3.2.4 Flight Management for Auto Position Hold

System not used.

#### 3.2.5 Cage Design & Tether

# Experimental Results

## 4.1 Stationary Propulsor Test

#### 4.1.1 Comparison of Vortex Distributions

#### 4.1.2 Version 1.0 EDF

Heavy Blue: 3 exits and 3 rotor vortex designs. Comparison of intake performance (long and short).

- Power (Current and Voltage)
- Thrust
- FOM
- RPM

#### 4.1.3 Version 2.0 EDF

1 exit and 2 rotor vortex designs. Long intake only.

- Power (Current and Voltage)
- Thrust
- FOM
- RPM
- Pressures

#### 4.1.4 Version 3.0 EDF

1 exit and 1 rotor vortex designs. Long intake only.

- Power (Current and Voltage)
- Thrust
- FOM
- RPM
- P1 Only

#### 4.1.5 Propeller

### 4.2 Hover Tests

#### 4.2.1 Propeller Performance

#### 4.2.2 Hover Test Limitations

## Future Work

Future work can be a proper section
Do the hover tests
Manoeuvre tests
- Look at what the Mf vs manoeuvre metric would look like
- What could the manoeuvre metric look like?
Actual theory on contra-rotating

### 5.1 Propulsor Design

#### 5.1.1 Stationary Propulsor Tests

What else would I have done to finish these off?

#### 5.1.2 Contra-rotating Ducted Fan

Motivation for CR design More smaller motors better? CAD of what it might look like. Velocity triangles ie Do the design and see how it would work theoretically.

#### 5.1.3 Computational Fluid Dynamics

- Discuss limitations of design method (with respect to previous sections on deviation etc.
- Reference Megs work? Show that CFD can get close to experimental results ie prove the method.

### 5.2 Flying Test Bed Experiments

How to quantify manoeuvre stability? The 'Eriksen' manoeuvre?

# Conclusions

# Appendix A: COVID-19

# Temporary Appendix Figures

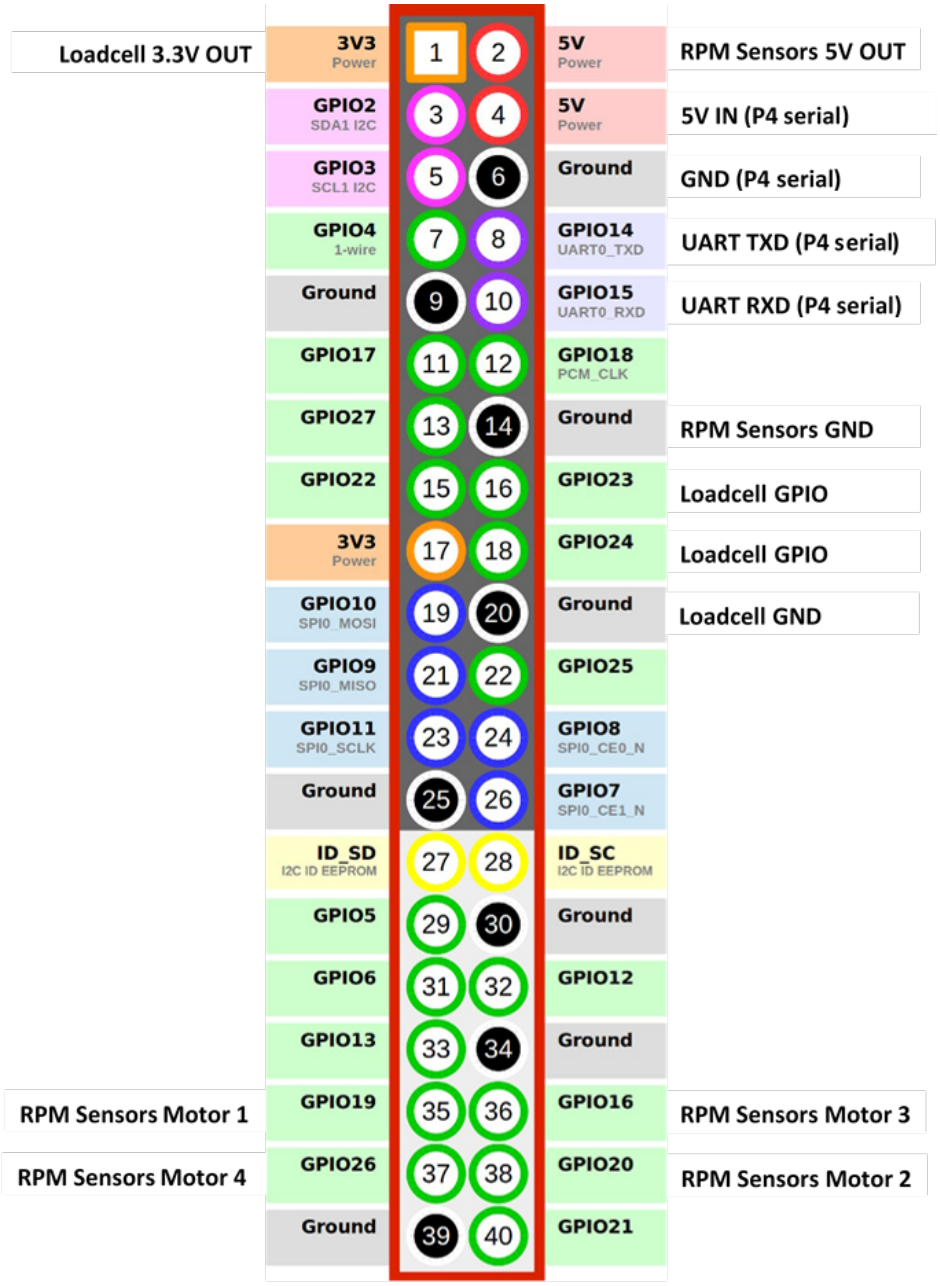


Figure 9: RPi3 header board with labelled used pins

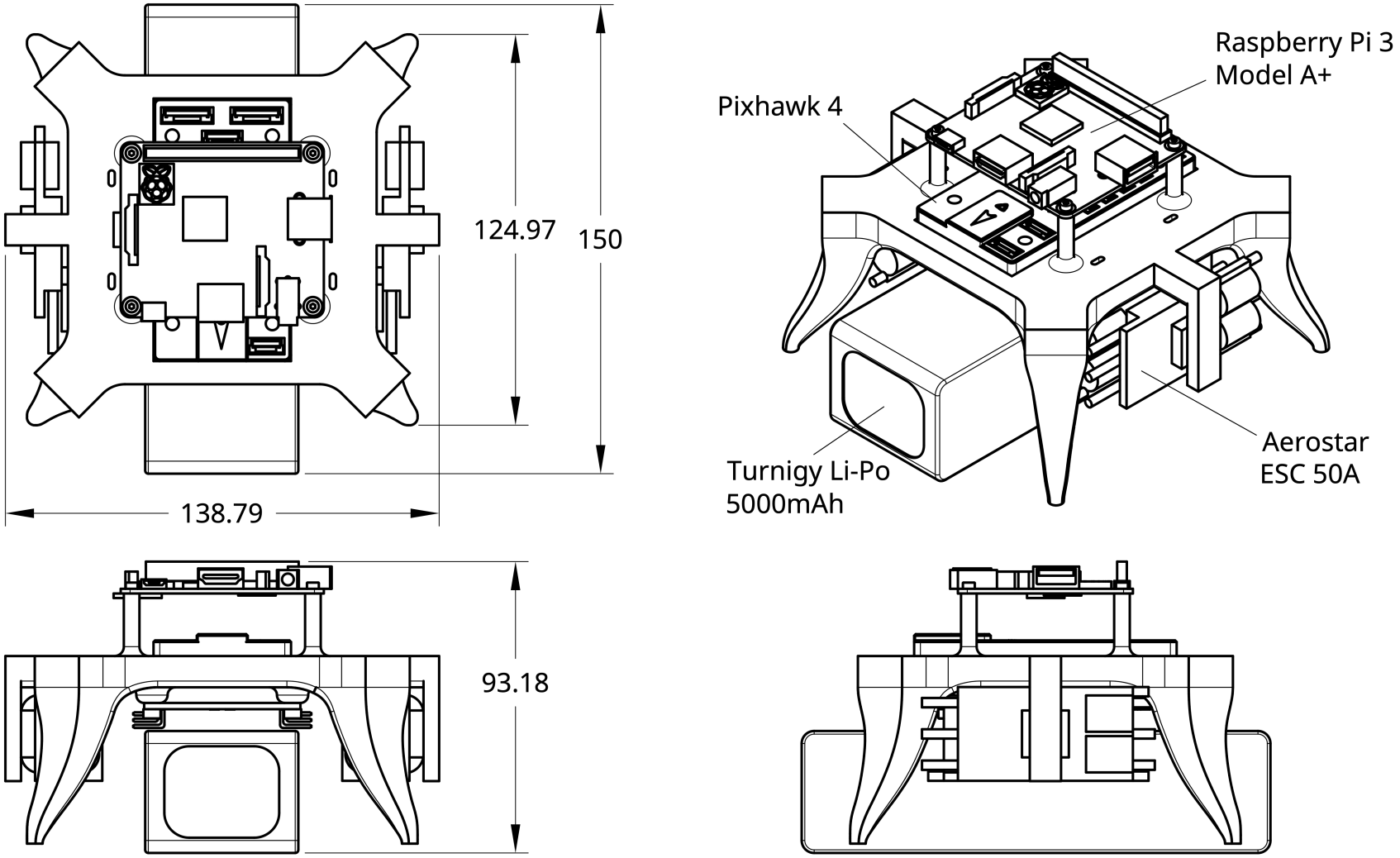


Figure 10: 3rd Angle projection of flying test bed chassis with principal dimensions and an isometric view